Journal of Materials Chemistry A

Gradient Porosity Electrode for Fast Charging Lithium-Ion Batteries

Journal:	*Journal of Materials Chemistry A*
Manuscript ID	TA-ART-03-2022-001707.R1
Article Type:	Paper
Date Submitted by the Author:	29-Apr-2022
Complete List of Authors:	Yang, Jian; Western Michigan University Li, Yejing; Argonne National Laboratory Mijailovic, Aleksandar; Brown University Wang, Guanyi; Western Michigan University Xiong, Jie; Western Michigan University Mathew, Kevin; Western Michigan University Lu, Wenquan; Argonne National Laboratory Sheldon, Brian; Brown University, Engineering Wu, Qingliu; Western Michigan University,

Gradient Porosity Electrode for Fast Charging Lithium-Ion Batteries

Jian Yang[a], Yejing Li[b], Aleksandar Mijailovic[c], Guanyi Wang[a], Jie Xiong[a], Kevin Mathew[a], Wenquan Lu[b,*], Brian W. Sheldon[c*], Qingliu Wu[a,*]

a- Department of Chemical and Paper Engineering, Western Michigan University, 4601 Campus Drive, Kalamazoo, Michigan, 49008-5462, U. S.A.

b- Chemical Science and Engineering Division, Argonne National Laboratory, 9700 South Cass Ave., Lemont, Illinois, 60439-4837, U. S. A.

c- School of Engineering, Brown University, 184 Hope St., Providence, Rhode Island, 02912, U. S. A.

* Correspondence should be addressed to:

Wenquan Lu; email: wenquan.lu@anl.gov; Phone: 630-252-3704, Fax: 630-252-4176

Brian W. Sheldon; email: brian_sheldon@brown.edu; Phone: 401-863-2866

Qingliu Wu, email: qingliu.wu@wmich.edu; Phone: 269-276-3998; Fax: 269-276-3501

Abstract: The tendency of Li plating at the surface of thick graphite electrodes greatly limits its application in electrical vehicle (EV) batteries for fast charging applications. To address this concern, we innovatively proposed a gradient porosity architecture to facilitate mass transport and suppress the Li plating in the thick anodes for fast charging applications. This concept was approved through a thick 3-layered graphite electrode with the highest porosity in the top layer and lowest porosity in the bottom layer, contacting with the current collector. The gradient porosity structure in the 3-layerd graphite electrode was confirmed by electron microscope and mercury porosimetry measurements. Used as the anodes of lithium-ion batteries, 3-layered graphite electrode demonstrated unprecedentedly superior rate capability and durability over 1-layered electrode. The post-mortem analysis on the cycled cells shows that 3-layered electrode could significantly suppress the Li plating at the high rate up to 4C, which might be responsible for the derived cells with improved performance. The excellent electrochemical behaviors of 3-layered graphite electrode are associated with the favored mass transport originated from the unique gradient porosity structure. This is in consistent with the theoretical studies that the introduction of the gradient porosity lowers Li-ion concentration gradient in the electrolyte in the region close to the separator and slows down the process to reach the threshold value of Li plating.

Key words: fast charge, graphite electrode, gradient porosity, lithium plating

1. Introduction

The rapid growth of global electrical vehicles (EVs) market requires lithium-ion batteries (LIBs) with both high-energy density and fast-charging capabilities[1]. However, the rate to charge the current high-energy EV batteries is limited due to adverse battery performance and safety issues at high current densities[2]. The main culprit of this limitation is the inevitable Li plating on the graphite[1, 3] at high rates, which is predominately used anode materials in state-of-art (SOA) LIBs[4]. The Li plating on graphite occurs when the charging rate exceeds diffusion rate of Li^+ within the graphite electrode[5], particularly for thick electrodes at high current densities[6, 7]. The formation of metallic Li on the graphite anode surface can cause irreversible lithium loss, rapid capacity fade, electrolyte decomposition, internal micro-short and other deleterious effects[6].

The key to realize fast charging LIBs lies in reducing the anode polarization to have anode potential above that for Li plating[2]. The concentration polarization, along with the charge-transfer overpotential and ohmic voltage drop, drives the anode potential below the thermodynamic potential of Li metal (<0 V versus Li^+/Li), leading to the Li plating at the surface of graphite[3]. Surficial coating with Al_2O_3[8], MoO_x-MoP_x[9], and graphene[10], and treatment with acid and base[11] could effectively reduce the charge-transfer impedance through facilitating Li-ion and/or electron transport at the surface of graphite particles. The ohmic voltage drop could be reduced through the employment of electrolytes with high Li^+ transference number[12, 13], selection of electrode materials[14],electrode design with high electronic conductivity[15] and utilization of separators with high electrolyte uptake[16, 17]. Both approaches could improve the intercalation kinetic process but have a limited effect in improving the sluggish Li^+ transport across the electrodes. In fact, the mass transport

within a graphite anode plays a decisive role in determining how fast a cell could be charged[18], especially at high rates in electrodes with high mass loadings[19].

Constructing electrodes with designed porous architectures is an effective way to improve the mass transport and mitigate the Li plating[17]. During the fast charge operation, the Li^+ transport limitation will inevitably establish a concentration gradient within the graphite anode, leading to a spatially inhomogeneous charging current[20, 21]. The energy dispersive X-ray diffraction measurement on a thick graphite electrode reveals that the LiC_6 phase accounts for all Li present at the electrode/separator interface and its concentration exponentially falls towards the current collector under certain charging conditions[22]. This Li inhomogeneity might lead to the Li plating in the region close to the electrode surface and the Li-starving region close to the current collector when we charge thick electrodes at high rates[22, 23]. All these observations imply that, compared with other regions, the region close to the electrode surface plays a more critical role in Li plating in anodes. Introducing a secondary porous network (SPN) with pore channels perpendicular to the current collector could facilitate the electrolyte transport through the whole the electrode and effectively suppress the Li plating within graphite anodes even at high rates. Successful examples include laser-structured graphite electrodes with patterned pores[5, 24, 25], freeze-casted graphite electrodes with lamellar porous structure[26, 27] and magnetically aligned graphite electrodes with graphite flakes aligned in the out-of-plane direction[28]. Despite of effectiveness of SPN, it is challenging to successfully and economically create SPN in the electrodes.

An alternative approach to address this concern is to introduce a varied porosities into the thick graphite electrode for fast charging LIB applications. The varied porosities

could enhance the electrolyte infiltration, decline the polarization and increase the utilization of active materials in the thick electrodes[29, 30]. Regardless of the critical role of anode in fast charge applications, most research on the gradient porosity, however, has been reported on the cathodes[31, 32] with using small particles in the top layer and large particles in the bottom layer to construct a bi-layered electrode to improve rate capabilities[33]. However, it is unclear that the improved rate performance is the result of the gradient porosity feature or utilization of small particles. In further, investigations on the anodes with varied porosity have been rarely reported and their role in LIBs at high rates is still uncertain[29, 30].

In this work, we firstly propose to establish a gradient porosity architecture to improve the mass transport and suppress the Li plating in a thick anode for the fast charge applications. This concept will be validated through a thick 3-layered electrode containing the same graphite but various porosity in every layer. The high loading 3-layered graphite electrode was fabricated through a facile approach, three-repeat conventional bar coating method. The thick graphite electrode has the highest porosity in the region close to the surface and the lowest porosity towards the current collector. The high porosity could favor the mass transport of electrolyte and thus alleviate Li plating in the region close to the graphite electrode surface. Compared with conventional electrodes with a high and uniform porosity, the gradient porosity electrode has the advantage of lower overall porosity and consequently higher areal mass loading. The superiority of the gradient porosity electrode in improving the battery performance over traditional electrodes with uniform porosity will be demonstrated.

2. Experimental

2.1. Electrode fabrication and cell assembly

Graphite (D_{50} of 16.9 μm and D_{90} of 26.7 μm, Targray), polyvinylidene difluoride (PVDF 9130, Kureha) and carbon black (100-200 nm, Super C45, MSE Supplies) were used as received without any modification or further treatment. Graphite and carbon black powders were dispersed in the binder solution with PVDF dissolved in N-Methylpyrrolidone (NMP) and well mixed by using a mixer (Thinky 100) to get a uniform slurry. The same slurry was used to fabricate both 1- and 3-layered electrodes.

A graphite electrode with gradient porosity feature could be fabricated through a facile approach involving repeated bar coating followed by pressing, as shown in **Figure 1**. For bottom layer coating, the well mixed slurry was casted onto the Cu foil and then dried in vacuum oven at 80 °C for 12 h. The dried coating was calendered to a thickness to meet the targeted porosity. The same approach was repeated to coat the second layer (middle layer) on the bottom layer, and third layer (top layer) on the middle layer. Every layer was pressed to a thickness to achieve the targeted porosities of 15% for bottom layer, 25% for middle layer and 35% for top layer. The final 3-layered electrodes had an overall porosity of ~25%, which is generally applied to electrodes with moderate areal capacities for EV applications[17]. The 10% difference made it feasible to generate different porosities in neighbored electrode layers during the electrode fabrication and to distinguish the porosity changes along the thickness direction in the final electrodes under the inspection. The same approach was used to produce the 1-layered electrode with a single laminate on the Cu foil, and the dried coating was calendered to have a same and uniform porosity of ~25%. Both dried 1- and 3-layered electrodes had the same mass loading of ~ 9 mg/cm^2

and were composed of 92% graphite, 2% carbon black and 6% PVDF. The physical properties of both 1-layer and 3-layer electrodes are detailed in **Table S1**.

2.2. Characterizations

2.2.1. Material and electrode characterizations

Morphology and surface: Scanning electron microscope (SEM) and Energy dispersive spectroscopy (EDS) were performed on a JEOL IT-200 InTouch microscope at 20 kV to collect information about the morphological and surficial information about the pristine and cycled electrodes. Before SEM observations, the cells underwent rate tests were charged (delithiated) to 1.5V and disassembled inside the glovebox. The harvested electrodes were carefully rinsed by the ethyl methyl carbonate (EMC) and dried.

Mercury intrusion/extrusion: Mercury Porosimetry characterization was conducted at MSE Supplies LLC using a Micromeritics' AutoPore V 9600. The measurements were performed with a penetrometer of 5.9 ml bulb volume and 0.392 ml stem volume. For the sake of accuracy, a sample weight of 0.4-0.5 g (~30 pieces of 1.6 cm^2 coated electrode pieces) was added to the penetrometer. The data were collected within a pressure (P) range of 0-420 MPa. Pore diameters were calculated assuming pores with a cylindrical shape and mercury-graphite contact angles of 130° to determine the pore size distribution (PSD). The porosity of electrode coating ($\varepsilon_{coating}$) was calculated through following equation (1):

$$\varepsilon_{coating} = \frac{V_{pore}/m_{coating}}{V_{coating}/m_{coating}} = \frac{V_{pore}/m_{coating}}{\dfrac{V_{coating}}{m_{sample} \times (1 - w_{Cu}\%)}} \quad (1)$$

Where $V_{coating}$, $m_{coating}$, m_{sample} and $w_{Cu}\%$ are the volume of coating, mass weight of coating, mass weight of electrode sheet and mass weight percentage of Cu foil in the

electrode sheet respectively. It is noted that pore volume (V_{pore}) did not include the volume contribution from pores with diameter of >30 μm, which is larger than D_{90} of graphite particles used here[32].

2.2.2. Electrochemical characterizations

The prepared graphite electrodes were cut into disks of 1.6 cm^2 and assembled in 2032-type coin cells with lithium metal as counter electrodes. The solution containing 1.2 mol/L $LiPF_6$ in ethylene carbonate (EC)/EMC (3/7 by weight) was used as the electrolyte. All cells were assembled inside the glovebox.

Formation: Galvanostatic cycling tests of all assembled cells were conducted on a Neware BTS4000 at a constant current of C/10 over the voltage range from 1.5 V to 0.01 V at room temperature. After 3 formation cycles, cells were divided into three groups for further electrochemical investigations. The cycling test was applied to one group of cells, and rate tests for the rest two group cells.

Rate capability: After 3 formation cycles, two types of rate tests were conducted on two groups of cells respectively. For the first group of cells, the constant current-constant voltage (CC-CV) mode was applied to both charge (delithiation) and discharge (lithiation) processes. A constant current of C/3 was used to delithiate the cells to 1.5 V followed by voltage hold at 1.5 V until the current below C/20 or the total delithiation time reached 3 hours. An incremental current density (C/10, C/2, 1C, 2C and 4C) was applied to the lithiation processes. At every rate, the cells were lithiated to 0.01 V with a constant current density followed by voltage hold at 0.01 V until current density below C/20 or the overall lithiation time reached the time corresponding to the rate. For the second group of cells, the same CC-CV mode was applied to the lithiation processes, but, at every rate, the cells

were lithiated to 80% state-of-charge (SOC) without controlling the cutoff voltage. At every rate, the cells underwent three cycles.

Cycling test: After 3 formation cycles, the cycling test was conducted on the third group of cells. The CC-CV mode was applied for the cycling test with the voltage window of 1.5 V-0.01 V. A constant current density of C/3 was used for the delithiation process, and 2C for the lithiation process.

2.3. Modeling

The half-cell rate capability experiments with cell lithiated to 80% SOC were modeled using the Newman pseudo-2D model implemented in COMSOL Multiphysics 5.6® software. A detailed description of the modeling equations and boundaries (e. g., current collector/graphite interface, graphite/graphite interface at different porosity regions) are described elsewhere[34]. A schematic of 1- and 3-layered model is shown in **Figure 8a**. These were described with a 1D geometry in the numerical model, using the parameters listed in the **Table S2-4** (including the physical properties of 1.2 M $LiPF_6$ in EC/EMC (w/w, 3/7), graphite, and Li metal interface kinetics). The only difference in parameters between the 1- and 3-layered models was the porosity in each region and corresponding tortuosity (which alters local effective ionic conductivity and effective diffusivity of the solid phase). The criteria for lithium metal plating were set with the lithium overpotential

$$\eta_{Li} = \phi_s - \phi_l \leq 0 \qquad (2)$$

where ϕ_l is the potential in the liquid phase and ϕ_s is the potential in the solid phase. These values correspond to conditions where metallic Li formation is thermodynamically allowable.

3. Results and Discussion

Using a facile approach shown in **Figure 1**, a gradient porosity feature could be established in a laminated electrode with the porosity of each layer well controlled. This could be confirmed by the SEM observations on 1- and 3-layered graphite electrodes (**Fig. 2**). Compared with 1-layered electrode (**Fig. 2a**), the 3-layered electrode (**Fig. 2c**) has a rougher surface with more loosely packed graphite particles. The loosely packing of particles is in consistent with the relatively higher porosity of top layer in 3-layered electrode (35%) than that across the 1-layered electrode (25%). In the scope of inspection, observations on the cross section (**Fig. 2d**) demonstrate the compaction degree varied along the thickness in the 3-layered graphite electrode: a dense layer near the current collector (bottom layer, ~32 μm), relatively loose middle layer (~36 μm) and the most loose top layer (~36 μm). On the contrary, the 1-layered graphite electrode shows a uniform and isotropic compaction degree without obviously and relatively dense and/or loose layers observable across the whole electrode (**Fig. 2b**). Given the same graphite and carbon black used for every laminate, the variety of compaction degree will build a gradient porosity across the 3-layered electrodes and the pore size distribution, which will be discussed below.

The establishment of gradient porosity could be further verified by the porosity analysis on the 3-layered graphite electrode. **Figure 3a** shows the mercury intrusion and extrusion porosimetry curves for 1- and 3-layered graphite electrodes. Regardless of the porous structure, the intrusion curves of both electrodes demonstrate a slop followed by a plateau in the low-pressure region of <0.04 MPa, characteristic of large pores (>30 μm) constructed by packed electrodes pieces[35, 36]. From the middle to high pressure, the

intrusion curve of both electrodes shows a three-step incremental changes followed by a horizontal plateau at high pressure, indicative of the variety of pore size distribution in the electrodes. This could be corroborated by the analysis on the pore size distribution (PSD).

Figure 3b shows that the PSD of the 1-layered electrode can be partitioned into two characteristic pore size regions, one for medium pores (60 nm < pore diameter < 550 nm) with a peak at ~202 nm and the other for large pores (550 nm < pore diameter < 4.8 μm) with a peak at ~1.4 μm. Assuming that pores are tetrahedral ($D_{void} = 0.225\ D_{50,\ particle}$) and octahedral voids ($D_{void} = 0.414\ D_{50,\ particle}$) in a close packing of spherical particles, the agglomerates of graphite particles ($D_{50} = 16.9$ μm) will generate pores with the diameter in the range of 3.8-7.0 μm. Given that the electrodes were heavily calendered, it is reasonable to consider that large pores are associated with the voids in the graphite matrix and the medium pores are from the graphite/carbon black mixture matrix. Besides large- and medium-pore regions, the PSD of 3-layered electrode shows an additional region with small pores (pore diameter < 60 nm). In addition, the 3-layered electrode has a broader large-pore region with an additional peak at ~2.5 μm. The small pores could be ascribed to the voids in the agglomerates of carbon black particles with the same assumption for packing graphite particles. The emergence of small pores implies that the electrode coating was highly compressed, leading to the close packing of small carbon black particles and low porosity. The broader large-pore region with a larger pore size indicates that the electrode coating had particles loosely packed and thus high porosity. In other words, low and high porosities coexist in the 3-layered electrode. This is in consistent with the structure constructed in the 3-layered electrode, which has a compacted bottom layer with a low

porosity of ~15% and loose top layer with a high porosity of ~35%, while 1-layered electrode merely has one coating with uniform and same porosity of ~25%.

Gradient porosity electrode has comparable battery performance in terms of specific capacity and irreversible capacity loss (ICL). **Figure 4** shows that both 1- and 3-layered electrodes exhibit almost identical discharge (lithiation) curves with a slope feature above 0.25 V followed by three plateaus at ~ 0.25, ~0.15 and ~0.05 V, characteristics of the lithiation of graphite. The specific capacity delivered by both 1- and 3-layered electrodes is almost same as ~350 mAh/g (delithiation capacity in the 3rd formation cycle). Both electrodes have almost same ICL, which is ~6% in the initial cycle, greatly drops to ~1% in the 2nd cycle and slightly reduced to ~0.8% in the 3rd cycle. The consistent electrochemical performance of 1- and 3-layered graphite electrodes suggests minimal effort of electrode pore structure when they were cycled at low charge and discharge rate.

The benefit of gradient porosity feature on the transportation of Li ions across the graphite electrode could be observed from the fast-charging and cycling tests. When the lithiation processes were terminated at the same cut-off voltage 10 mV, the 3-layered electrodes showed almost overlap voltages and delivered almost identical capacity with those from 1-layered electrodes (**Fig. 5a**). However, the 3-layered electrode demonstrates slightly higher capacity during the delithiation processes, especially at higher rates (**Fig. 5b**). This implies that the gradient porosity could effectively improve the coulombic efficiencies of cells. More important, the electrode with the gradient porosity feature demonstrates the unprecedently superior cycle life over that with homogeneous porosity (**Fig. 5c**). The 3-layered electrode retains the high capacity of 125 mAh/g after 150 cycles, when the cells were lithiated (discharged) at 2C rate. However, less than 50 mAh/g is

retained in the 1-layered electrode after merely ~50 cycles. In addition, the coulombic efficiency of 1-layered electrode drops to <99% after 50 cycles, but it is still higher than 99% for 3-layered electrodes even after 150 cycles. The lower coulombic efficiency implies that the lithium dendrite, or "dead" lithium, accumulated in the 1-layered electrode, leading to fast capacity decay.

The superiority of gradient porosity structure in suppressing Li plating could be validated through the post-mortem analysis on the electrodes harvested from the cells underwent 4C rate tests with the lithiation cut-off voltage of 10 mV. **Figure 6** shows spherical graphite particles observable at the top surface of both 1- and 3-layered electrodes (**Fig. 6b** and **6d**). A large amount of white agglomerates, which are composed of numerous small particles with irregular shape and wide range of size, could also be observed at the surface of the 1-layered electrode (**Fig. 6a**). On the contrary, bare white agglomerates could be found at the surface cycled 3-layered electrode (**Fig. 6c** and **6d**). The energy dispersive X-ray spectroscopy (EDS) mapping over the cycled 1-layered graphite electrode shows a representative white agglomerate is only composed of O element without detectable C, F or P elements (**Fig. 6e** to **6i**). The absence of C, F and P excludes the possibility that these white agglomerates are oxidized lithium salt from the residual electrolyte or solid electrolyte interface (SEI) formed at the surface of graphite electrodes during the lithiation/delithiation processes. It is highly possible that these white agglomerates come from plated Li metal particles, which were oxidized in the course of transferring samples to SEM chamber, although no Li element is identified due to its low-energy radiation characteristics. Apparently, the gradient porosity feature plays a crucial role in suppressing the Li plating in the thick graphite electrode. The greatly improved rate capability and cycle

life of batteries (**Fig. 5)** is the result of the suppressed Li plating in 3-layered electrodes[23], compared to those with 1-layered electrodes. It is worth to note that the cut-off voltage of 10 mV (vs. Li^+/Li) used here was slightly above the thermodynamic potential of Li metal (<0 V vs. Li^+/Li) at room temperature. However, the Li plating could take place above 0 V (vs. Li^+/Li) at a higher temperature[21]. The fast charge operation generally generates intensified heat[3, 37] and nonuniform temperature distribution within the electrodes[21]. Given the sluggish mass transport and consequently high polarization, it is rational to observe the locally plated Li metals at the surface of 1-layered graphite electrode after the fast charge operation with the cut-off voltage above 0 V (vs. Li^+/Li). However, the gradient porosity feature improves the mass transport and reduces the polarization within the electrode, predicted from our theoretical calculations (**Fig. 8**). Together with the high cut-off voltage of 10 mV, the 3-layered graphite electrode has the capability of suppressing the Li plating even at a high temperature after the fast charge operation.

It is clear that the promise of 3-layered electrodes in improving rate capability of LIBs is not fully manifested during cycling with shallow lithiation and a fixed cut-off voltage. The superior fast charging capability of 3-layered electrode is better validated by the results from the second type of rate test, where the terminated condition of 10 mV cut-off voltage was replaced by 80% of the graphite theoretical capacity in the lithiation process at all rates (**Fig. 7**). When the lithiation rates are less than 1C, the 1-layered electrode exhibits smooth voltage curves (**Fig. 7a**). However, there is a voltage dip around 200 mAh/g when the lithiation rate is 2C, and this voltage dip shifts to the lower SOC with increasing lithiation rates (4C and 6C) (**Fig. 7a**). As for the 3-layered electrodes, there is no voltage dip during the lithiation process until the lithiation rate is 4C. Furthermore, the

delithiaton capacities of the 3-layered electrode are 250 mAh/g at 2C, 150 mAh/g at 4C and 100 mAh/g at 6C, which are 1.13, 1.5 and 2 times higher than those of the 1-layered electrode at 2C, 4C and 6C respectively (**Fig. 7b**). Together with the less polarized voltage profile during high-rate lithiation, it is obvious that the 3-layered electrode has much better fast charging performance. In further, we believe that the voltage dip is indicative of the Li plating and the gradient porosity could effectively suppress the Li plating in the 3-layered graphite electrode at high rates, which will be discussed in the modeling below.

To better understand the role of gradient porosities in graphite electrode, theoretical simulations were conducted, and the results are shown in **Figure 8** for 1C and 4C lithiation rates, at the threshold for Li plating (i.e., when the local Li overpotential at the separator reaches zero). When this condition is reached, the local (average) SOC profile for the 3-layered electrode lies above the profile for the 1-layered electrode (**Fig. 8b**). This demonstrates that introducing gradient porosity improves the utilization of graphite and thus leads to the higher capacity in the 3-layered electrode at the plating threshold. This higher graphite utilization is ascribed to the faster ionic transport that occurs in the outer portions of the 3-layered electrode.This effect is also corroborated by the higher Li concentration in the middle layer of 3-layered electrode, especially at 4C (**Fig. 8c**). It is instructive to note that the Li-ion concentration in the 3- and 1-layered models do not correlate with the trend in local SOC, as the Li-ion concentration is higher near the separator and lower near the current collector for the 3-layered model, compared to 1-layered model (**Fig. 8c**). Furthermore, there is no Li-ion depletion in either model at these rates. The equilibrium potential, which is directly related to local surface SOC, is lower through the thickness of the cell for 3-layered case (**Fig. 8d**), which is consistent with the

trends in local SOC (**Fig. 8b**). This trend is also correlated with the difference in liquid potential (ϕ_l) profiles, between the 3- and 1-layered models (**Fig. 8e**). Specifically, the gradient porosity has more profound impact on the material utilization, tortuosity and diffusion length in the region near to the separator. Compared with 1-layered model, the increased porosity and, consequently, reduced tortuosity near the separator significantly lower the gradients in liquid potential are lower near the separator for the 3-layered case (**Fig. 8e**). Therefore, the improved ionic transport via increased porosity in the 3-layered electrode increases capacity at the plating threshold by reducing large gradients in the liquid potential and equilibrium potential near the separator. In other words, the 3-layered electrode has the region near the separator far away from the threshold for Li plating when it is lithiated to the same SOC as that of the 1-layered electrode. This is consistent with the results from our rate capability measurements with stable electrochemical performance and suppressed Li plating observed on the 3-layered electrodes (**Fig. 6** and **7**). It is worth to note that the gradient porosity feature enables graphite electrodes superior battery performance over those with uniform and homogeneous porosity. However, the porous structure of 3-layered electrodes constructed here is not optimal. The optimum configuration is highly dependent on parameters including material properties (e.g., ionic conductivity of the electrolyte, tortuosity correlation for a graphite material etc,), mass loading, porosity (and, consequently, tortuosity), thickness, and C-rate. These complexities make generalizing design strategies difficult (other than increasing porosity in the anode near the separator), and the optimization and guide to design of layered structures are treated in a separate work.[34]

4. Conclusions

A gradient porosity feature was successfully incorporated into a thick 3-layered graphite electrode. The gradient porosity feature facilitates the Li-ion transportation across the electrode, evidenced by the 3-layered graphite electrode with stable performance at the rate up to 4C, high capacity and coulombic efficiency. Furthermore, cells with 3-layered graphite electrode exhibit greatly improved cycle life, compared to those with 1-layered electrodes. The superior durability of 3-layered electrode over 1-layered electrode is associated with the significantly suppressed Li plating during numerously repeated lithiation/delithiation processes. The concept of gradient porosity for improving mass transport and mitigating Li plating and the facile approach of fabricating layered electrodes proposed here are of both scientific and practical significance in electrode design and manufacturing for fast charge applications.

Acknowledgments

This material is based upon work supported by the U. S. Department of Energy's Office of Energy Efficiency and Renewable Energy (EERE) under the Advanced Manufacturing Office, award number DE-EE0009111.

References

1. A. Tomaszewska, Z. Y. Chu, X. N. Feng, S. O'Kane, X. H. Liu, J. Y. Chen, C. Z. Ji, E. Endler, R. H. Li, L. S. Liu, Y. L. Li, S. Q. Zheng, S. Vetterlein, M. Gao, J. Y. Du, M. Parkes, M. G. Ouyang, M. Marinescu, G. Offer and B. Wu, *Etransportation*, 2019, **1**.
2. W. L. Cai, Y. X. Yao, G. L. Zhu, C. Yan, L. L. Jiang, C. X. He, J. Q. Huang and Q. Zhang, *Chem Soc Rev*, 2020, **49**, 3806-3833.
3. Y. Y. Liu, Y. Y. Zhu and Y. Cui, *Nat Energy*, 2019, **4**, 540-550.
4. K. G. Gallagher, S. E. Trask, C. Bauer, T. Woehrle, S. F. Lux, M. Tschech, P. Lamp, B. J. Polzin, S. Ha, B. Long, Q. L. Wu, W. Q. Lu, D. W. Dees and A. N. Jansen, *J Electrochem Soc*, 2016, **163**, A138-A149.
5. K. H. Chen, M. J. Namkoong, V. Goel, C. L. Yang, S. Kazemiabnavi, S. M. Mortuza, E. Kazyak, J. Mazumder, K. Thornton, J. Sakamoto and N. P. Dasgupta, *J Power Sources*, 2020, **471**.
6. P. C. Zhang, T. Yuan, Y. P. Pang, C. X. Peng, J. H. Yang, Z. F. Ma and S. Y. Zheng, *J Electrochem Soc*, 2019, **166**, A5489-A5495.
7. A. M. Colclasure, A. R. Dunlop, S. E. Trask, B. J. Polzin, A. N. Jansen and K. Smith, *J Electrochem Soc*, 2019, **166**, A1412-A1424.
8. D. S. Kim, Y. E. Kim and H. Kim, *J Power Sources*, 2019, **422**, 18-24.
9. S. M. Lee, J. Kim, J. Moon, K. N. Jung, J. H. Kim, G. J. Park, J. H. Choi, D. Y. Rhee, J. S. Kim, J. W. Lee and M. S. Park, *Nat Commun*, 2021, **12**.
10. Y. B. Mu, M. S. Han, J. Y. Li, J. B. Liang and J. Yu, *Carbon*, 2021, **173**, 477-484.
11. J. Kim, S. M. N. Jeghan and G. Lee, *Micropor Mesopor Mat*, 2020, **305**.
12. E. R. Logan and J. R. Dahn, *Trends Chem*, 2020, **2**, 354-366.
13. S. S. Zhang, *Infomat*, 2021, **3**, 125-130.
14. C. Heubner, K. Nikolowski, S. Reuber, M. Schneider, M. Wolter and A. Michaelis, *Batteries Supercaps*, 2021, **4**, 268-285.
15. Y. X. Tang, Y. Y. Zhang, W. L. Li, B. Ma and X. D. Chen, *Chem Soc Rev*, 2015, **44**, 5926-5940.
16. D. Parikh, T. Christensen, C. T. Hsieh and J. L. Li, *J Electrochem Soc*, 2019, **166**, A3377-A3383.
17. J. L. Li, J. Fleetwood, W. B. Hawley and W. Kays, *Chem Rev*, 2022, **122**, 903-956.
18. C. Birkenmaier, B. Bitzer, M. Harzheim, A. Hintennach and T. Schleid, *J Electrochem Soc*, 2015, **162**, A2646-A2650.
19. Z. J. Du, D. Wood, C. Daniel, S. Kalnaus and J. L. Li, *J Appl Electrochem*, 2017, **47**, 405-415.
20. P. P. Paul, V. Thampy, C. T. Cao, H. G. Steinruck, T. R. Tanim, A. R. Dunlop, E. J. Dufek, S. E. Trask, A. N. Jansen, M. F. Toney and J. N. Weker, *Energ Environ Sci*, 2021, **14**, 4979-4988.
21. H. S. Wang, Y. Y. Zhu, S. C. Kim, A. E. Pei, Y. B. Li, D. T. Boyle, H. X. Wang, Z. W. Zhang, Y. S. Ye, W. Huang, Y. Y. Liu, J. W. Xu, J. Li, F. Liu and Y. Cui, *P Natl Acad Sci USA*, 2020, **117**, 29453-29461.
22. K. P. C. Yao, J. S. Okasinski, K. Kalaga, I. A. Shkrob and D. P. Abraham, *Energ Environ Sci*, 2019, **12**, 656-665.
23. A. S. Ho, D. Y. Parkinson, D. P. Finegan, S. E. Trask, A. N. Jansen, W. Tong and N. P. Balsara, *Acs Nano*, 2021, **15**, 10480-10487.

24. L. Kraft, J. B. Habedank, A. Frank, A. Rheinfeld and A. Jossen, *J Electrochem Soc*, 2019, **167**.
25. J. B. Habedank, J. Kriegler and M. F. Zaeh, *J Electrochem Soc*, 2019, **166**, A3940-A3949.
26. R. Amin, B. Delattre, A. P. Tomsia and Y. M. Chiang, *Acs Appl Energ Mater*, 2018, **1**, 4976-4981.
27. F. L. E. Usseglio-Viretta, W. Mai, A. M. Colclasure, M. Doeff, E. Yi and K. Smith, *Electrochim Acta*, 2020, **342**.
28. J. Billaud, F. Bouville, T. Magrini, C. Villevieille and A. R. Studart, *Nat Energy*, 2016, **1**.
29. S. Kalnaus, K. Livingston, W. B. Hawley, H. Wang and J. L. Li, *J Energy Storage*, 2021, **44**.
30. M. Wood, J. N. Li, Z. J. Du, C. Daniel, A. R. Dunlop, B. J. Polzin, A. N. Jansen, G. K. Krumdick and D. W. L. Iii, *J Power Sources*, 2021, **515**.
31. K. F. Song, C. Zhang, N. F. Hu, X. K. Wu and L. Zhang, *Electrochim Acta*, 2021, **377**.
32. L. Froboese, P. Titscher, B. Westphal, W. Haselrieder and A. Kwade, *Mater Charact*, 2017, **133**, 102-111.
33. A. N. Jansen, *eXtreme Fast Charge Cell Evaluation of Lithium-ion Batteries*, 2021, **BAT 456**.
34. A. Mijailovic, G. Wang, J. Yang, W. Lu, Q. Wu and B. Sheldon, *J Electrochem Soc*, 2022, **Submitted**.
35. D. Schreiner, T. Zund, F. J. Gunter, L. Kraft, B. Stumper, F. Linsenmann, M. Schussler, R. Wilhelm, A. Jossen, G. Reinhart and H. A. Gasteiger, *J Electrochem Soc*, 2021, **168**.
36. S. Radloff, L. S. Kremer, A. Hoffmann and M. Wohlfahrt-Mehrens, *Mater Today Commun*, 2021, **28**.
37. M. Keyser, A. Pesaran, Q. B. Li, S. Santhanagopalan, K. Smith, E. Wood, S. Ahmed, I. Bloom, E. Dufek, M. Shirk, A. Meintz, C. Kreuzer, C. Michelbacher, A. Burnham, T. Stephens, J. Francfort, B. Carlson, J. C. Zhang, R. Vijayagopal, K. Hardy, F. Dias, M. Mohanpurkar, D. Scoffield, A. N. Jansen, T. Tanim and A. Markel, *J Power Sources*, 2017, **367**, 228-236.

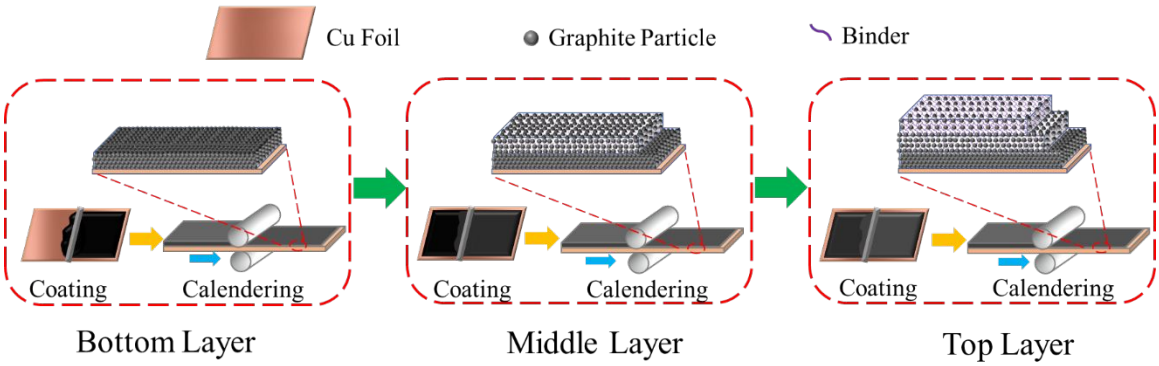

Figure 1. Schematic illustration of process to fabricate 3-layered electrodes with varied porosities along thickness direction.

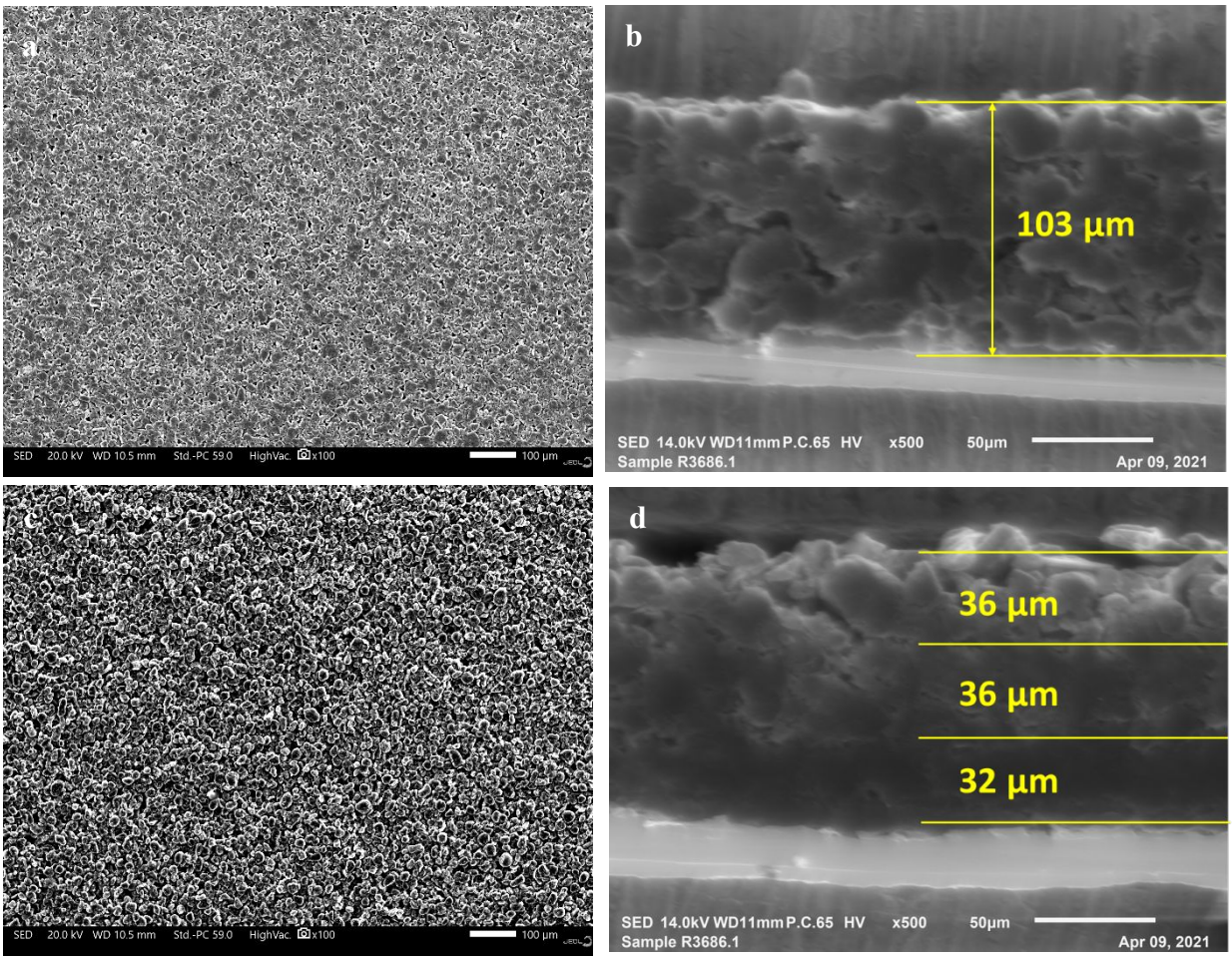

Figure 2. SEM images of top surface (a, c) and cross section (b, d) of 1-layered (a, b) and 3-layered (c, d) graphite electrodes.

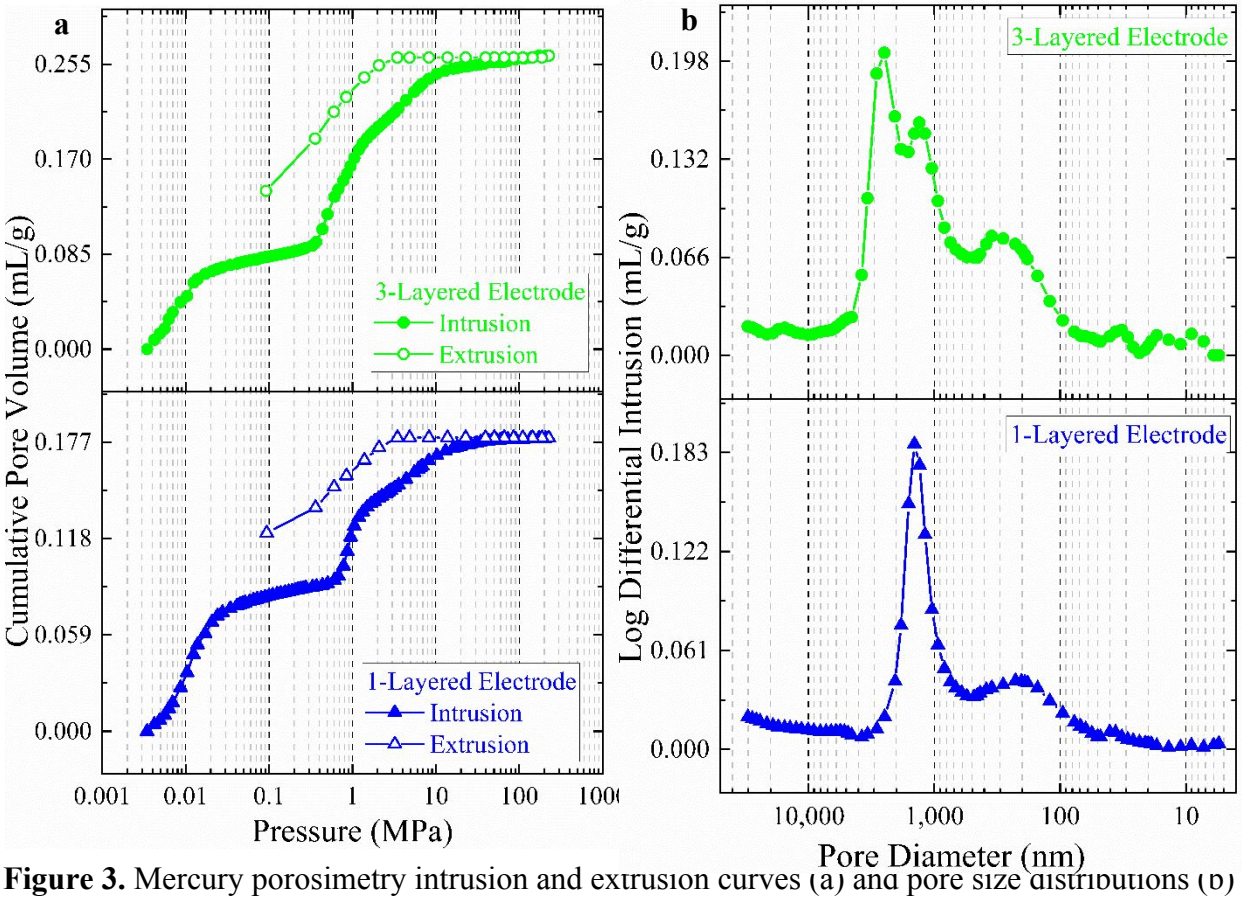

Figure 3. Mercury porosimetry intrusion and extrusion curves (a) and pore size distributions (b) of 1- and 3-layered graphite electrodes.

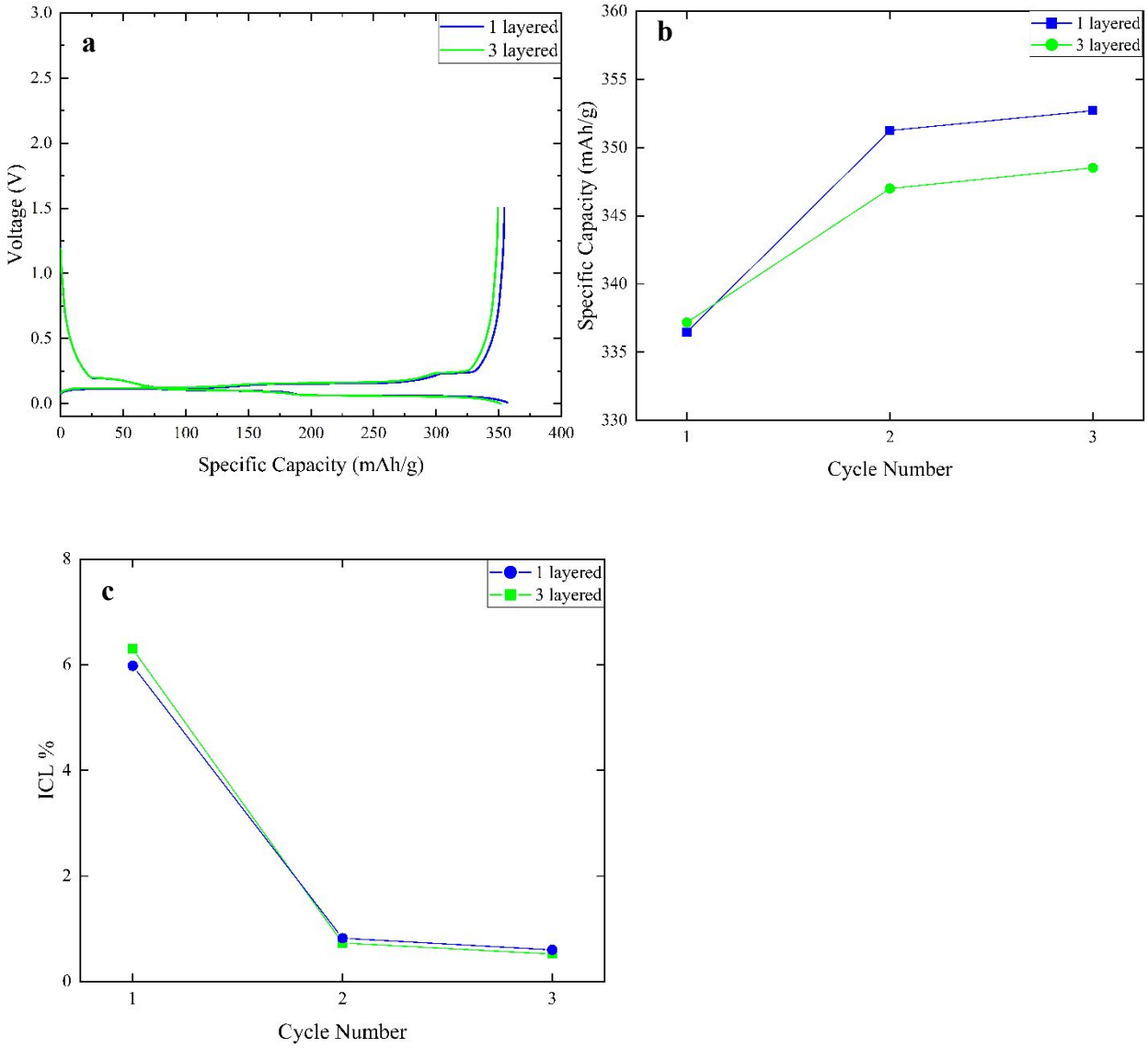

Figure 4. Voltage profiles (a) of 1- and 3-layered graphite electrodes during the third formation cycles. The specific capacity (b) and irreversible capacity loss (ICL, c) as a function of cycle number during the formation tests.

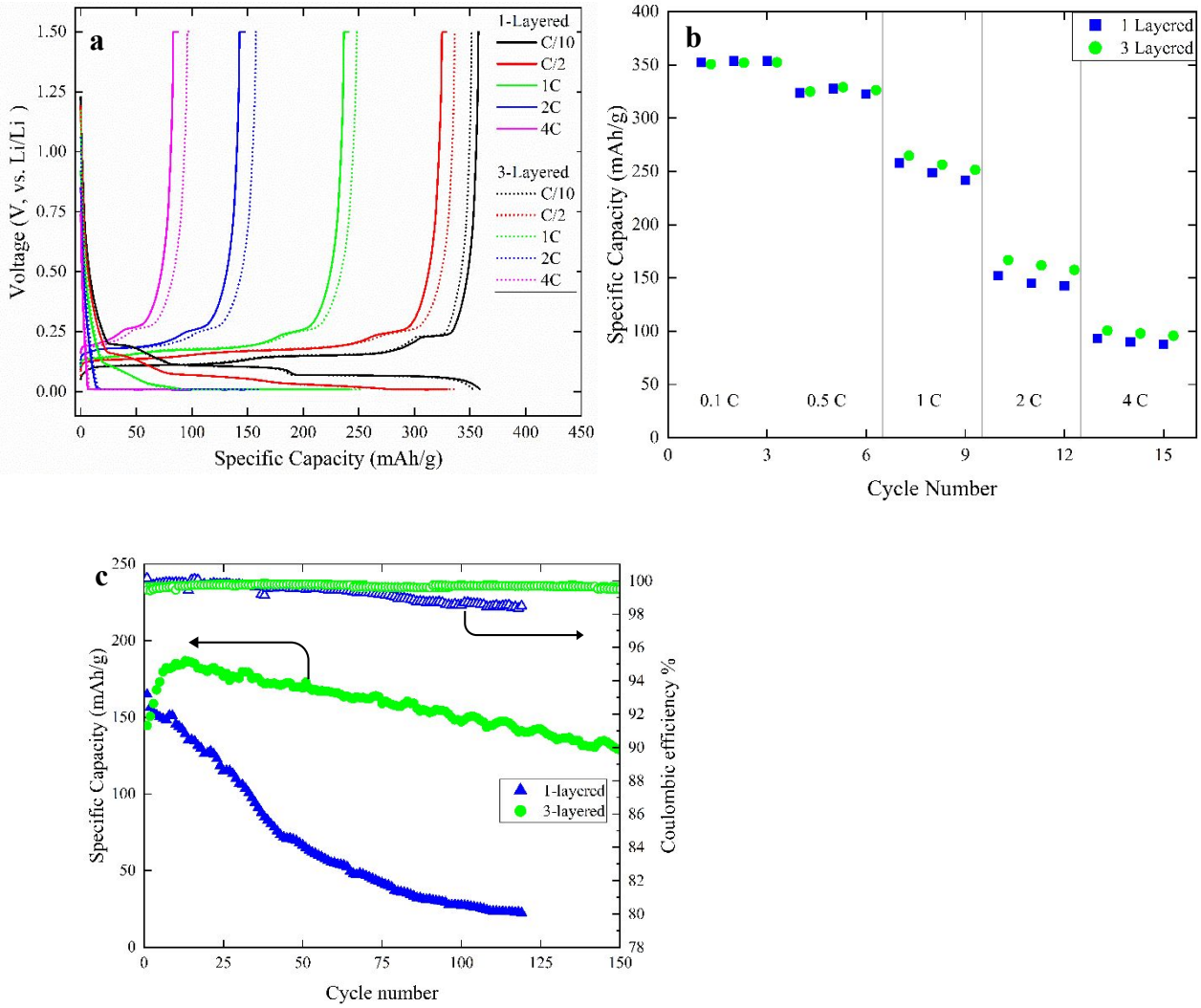

Figure 5. Voltage profiles (a), specific capacities (b) of 1- and 3-layered graphite electrodes with various fast-charging rates, and the cycling performance (c) of 1- and 3-layered graphite electrodes with 2C charging rate. The CC-CV mode was applied to both rate and cycling tests. At every rate, all cells were charged to 1.5 V, discharged to 10 mV and underwent three cycles. For comparison, the 3rd voltage profiles at every rate were plotted together. The specific capacities in (b) were averaged from three cells with 1- and 3-layered electrodes respectively. During the cycling test, a constant current density of C/3 was used for the delithiation process, and 2C for the lithiation process.

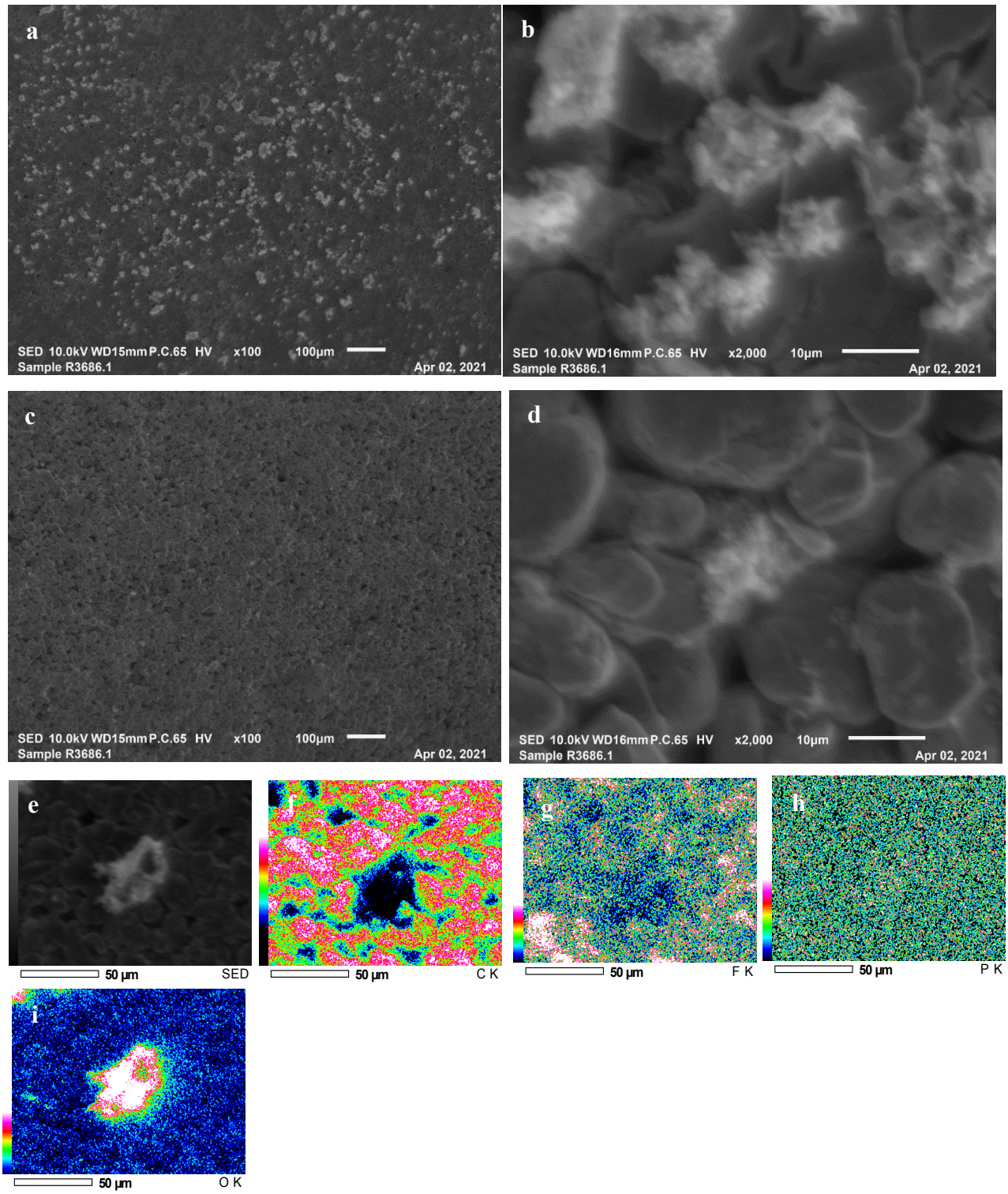

Figure 6. The low (a, c) and high (b, d) magnifications SEM images of cycled 1- (a, b) and 3- (c, d) layered graphite electrodes. The EDS mappings (e, f, g, h and i) of cycled 1-layered graphite electrodes. Both graphite electrodes were harvested from cells underwent 4C rate test with the cut-off voltage of 10 mV. All cells were delithiated to 1.5V before disassembly.

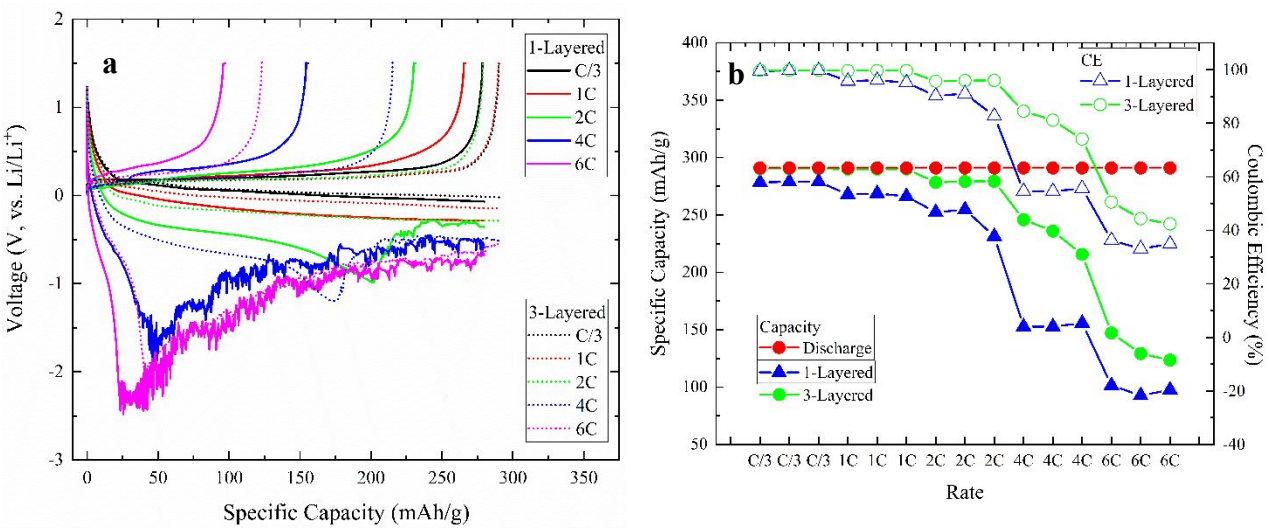

Figure 7. Voltage profiles (a) and capacities and coulombic efficiencies (b) of 1- and 3-layered graphite electrodes during rate tests. At every rate, all cells were charged (delithiation) to 1.5 V, discharged (lithiation) to 80% of the theoretical capacity and underwent three cycles. For comparison, the 3rd voltage profiles at every rate were plotted together.

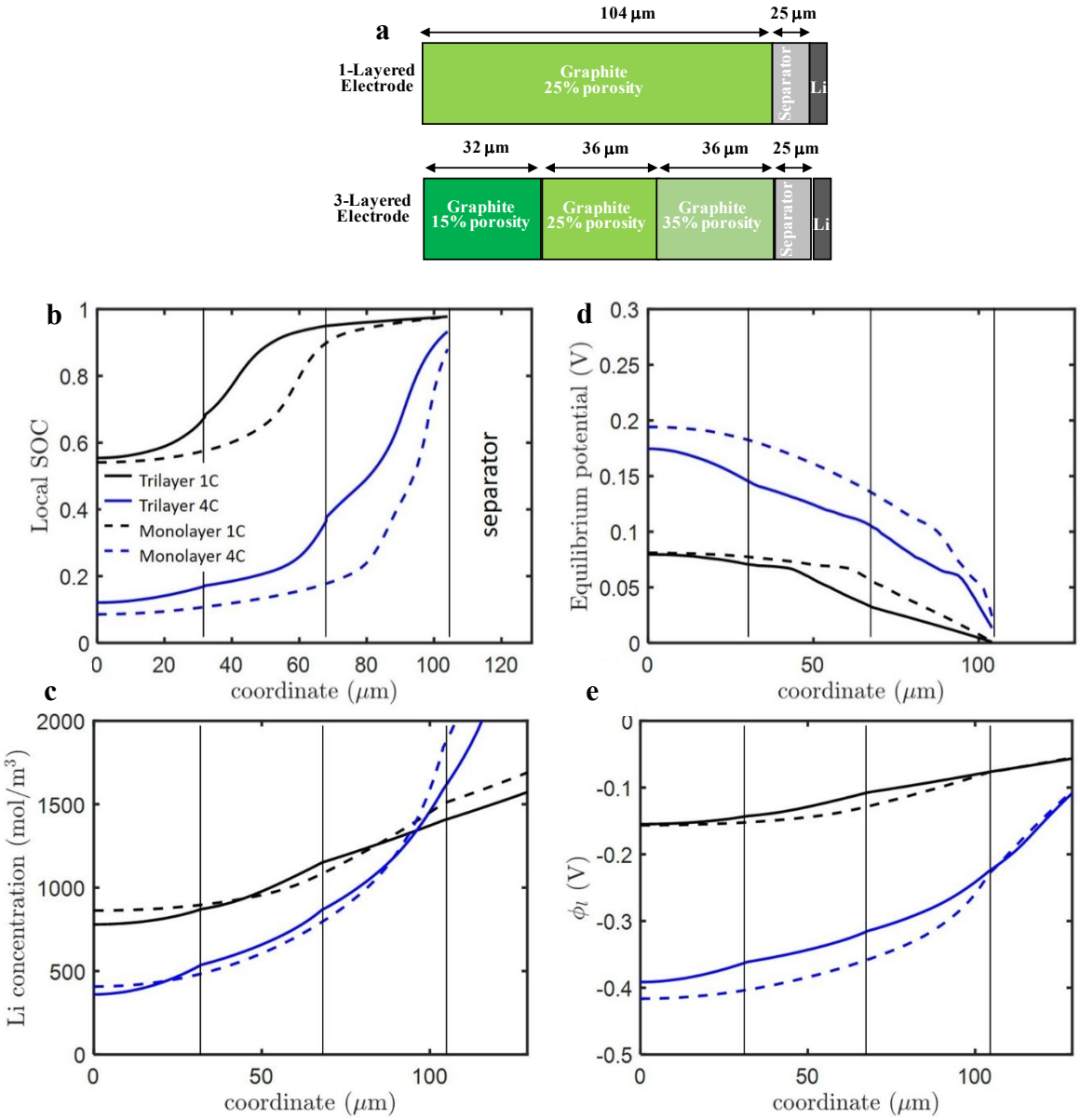

Figure 8. Schematic illustration (a) of 1- and 3-layered graphite cells used for simulation. The average local SOC (b), Li-ion concentration (c), equilibrium potential (d) and liquid potential (ϕ_l) (e) as a function of position in the electrode at the plating threshold at 1C (black) and 4C (blue) for 1- (dashed lines) and 3-layered electrodes (solid lines). The boundary for the electrode-separator interface and from low porosity to high porosity are indicated with vertical lines.